Research Square

Preprints are preliminary reports that have not undergone peer review.
They should not be considered conclusive, used to inform clinical practice,
or referenced by the media as validated information.

Design, Fabrication and Characterization of Microwave Multiplexing SQUID Prototype

Mengjie Song
Institute of High Energy Physics
Yixian Deng
Institute of High Energy Physics
Zhengwei Li
lizw@ihep.ac.cn

Institute of High Energy Physics
He Gao
Institute of High Energy Physics
Zhouhui Liu
Institute of High Energy Physics
Yudong Gu
Institute of High Energy Physics
XiangXiang Ren
Shandong University
Nan Li
Institute of High Energy Physics
Guofu Liao
Institute of High Energy Physics
Qinglei Xiu
Institute of High Energy Physics
Yu Xu
Institute of High Energy Physics
Mengqi Jiang
Institute of High Energy Physics
Xufang Li
Institute of High Energy Physics
Yaqiong Li
Institute of High Energy Physics
Shibo Shu
Institute of High Energy Physics
Yongjie Zhang

Institute of High Energy Physics

Congzhan Liu

Institute of High Energy Physics

Research Article

Keywords: microwave SQUID multiplexer, transition-edge sensor, RF-SQUID, cryogenic detector array readout

Posted Date: May 13th, 2026

DOI: https://doi.org/10.21203/rs.3.rs-9331414/v1

License: This work is licensed under a Creative Commons Attribution 4.0 International License. Read Full License

Additional Declarations: No competing interests reported.

Version of Record: A version of this preprint was published at Journal of Low Temperature Physics on August 20th, 2026. See the published version at https://doi.org/10.1007/s10909-026-03461-0.

Design, Fabrication and Characterization of Microwave Multiplexing SQUID Prototype

Mengjie Song[1,2], Yixian Deng[1,2], Zhengwei Li[1*], He Gao[1*], Zhouhui Liu[1], Yudong Gu[1], XiangXiang Ren[3], Nan Li[1], Guofu Liao[1], Qinglei Xiu[1], Yu Xu[1], Mengqi Jiang[1], Xufang Li[1], Yaqiong Li[1], Shibo Shu[1], Yongjie Zhang[1], Congzhan Liu[1*]

[1*]Key Laboratory of Particle Astrophysics, Institute of High Energy Physics, Chinese Academy of Sciences, Beijing, 100049, China.
[2]School of Physical Science, University of Chinese Academy of Sciences, Beijing, 100049, China.
[3]Key Laboratory of Particle Physics and Particle Irradiation(MOE), Institute of Frontier and Interdisciplinary Science, Shandong University, Qingdao, Shandong, 266237, China.

*Corresponding author(s). E-mail(s): lizw@ihep.ac.cn; hegao@ihep.ac.cn; liucz@ihep.ac.cn;

Abstract

The readout system with a high multiplexing ratio has become a bottleneck limiting the application of large-scale Transition Edge Sensor (TES) detector arrays. In recent years, the microwave superconducting quantum interference device (SQUID) multiplexer has emerged as a key technology for effectively reading large-scale cryogenic detector arrays. Currently, the microwave SQUID multiplexer is being adopted by an increasing number of experiments due to its capability of achieving a multiplexing ratio of 2000:1 within the readout bandwidth. In this study, we developed a 32-channel microwave SQUID multiplexer prototype. And we measured 8 channels of the prototype. The measured equivalent noise current of the prototype reached 154 pA/$\sqrt{Hz}$.

Keywords: microwave SQUID multiplexer, transition-edge sensor, RF-SQUID, cryogenic detector array readout

1 Introduction

The Transition-Edge Sensor (TES) is widely used in astronomical and cosmological observation experiments due to its extremely low noise. Absorption of photon energy or power causes a temperature change in the TES, which results in a significant change of its resistance. Usually, the normal resistance of a TES detector is designed ranging from several mΩ to tens of mΩ. It is hard to achieve noise impedance match with conventional semiconductor amplifiers, such as Junction Field-Effect Transistor(JFET). Superconducting Quantum Interference Device(SQUID) is nearly the only readout electronics option for TES [1]. By reducing the noise level while increasing the number of detectors, the observation sensitivity of millimeter wave/Cosmic Microwave Background(CMB) telescopes can be rapidly enhanced. The development of TES accelerates the upgrading and replacement of millimeter wave/CMB telescopes [2]. The increase in the number of detectors poses a significant challenge to the low-temperature readout technology of the TES array. Therefore, a multiplexing low-temperature readout technology needs to be employed to reduce the number of readout channels.

There are four main types of multiplexing low-temperature readout technology, which are Time Division Multiplexing (TDM) [3–6], Frequency Division Multiplexing (FDM) [7–9], Code Division Multiplexing (CDM) [10, 11], and microwave SQUID multiplexing(μMux) [12–15]. Among these techniques, TDM is the most widely employed, with a multiplexing ratio of typically around 64:1 in CMB observations[4]. TDM utilizes DC-SQUID and incorporates at least two stages in series. However, it has stringent requirements for yield. Conversely, FDM is constrained by its limited bandwidth, with TES operating in an AC bias state. The maximum multiplexing ratio of FDM for TES X-ray microcalorimeters reaches around 70:1 [8], and it may reach 170:1 in CMB observations. CDM can achieve a significantly high multiplexing ratio theoretically. However, a primary challenge associated with CDM is its complexity. As the array size increases, the complexity of the SQUID chip design and coding also escalates [10]. μMux employs the principle of frequency division multiplexing and utilizes radio-frequency SQUIDs (RF-SQUIDs) instead of DC-SQUIDs, thereby eliminating the need for series connections between DC-SQUIDs. This approach results in a considerable multiplexing ratio, currently reaching 1820:1 [15].

μMux has been selected as the readout electronics for various applications, including primordial gravitational wave detection and space X-ray astronomical telescopes, such as BICEP/Keck Array in South Pole [16], Simons observatory in Chile [17], Ali CMB Polarization Telescope(AliCPT) in China [18], the conceptual X-ray space mission Lynx [19], etc. AliCPT is the first primordial gravitational wave experiment in China, located in Ngari(Ali), Tibet. It has successfully achieved first light but currently operates with only one detector module. In the future, it is expected to be upgraded to 19 modules. For the upgrade of AliCPT, we designed a 32-channel μMux chip prototype for readout development. When the fabrication technology matures, the number of readout channel for each μMux is expected to increase to 80.

2 Design of the microwave SQUID multiplexer

The working principle of the μMux is illustrated in Fig.1. Each input channel consists of an RF-SQUID and a coplanar waveguide (CPW) quarter-wavelength resonator, with the resonator and RF-SQUID coupled through inductance. The resonators connect to a common readout CPW feedline through weak capacitive coupling. The RF-SQUID circuit functions as a quarter-wavelength transmission line load, effectively acting as a variable inductance. The equivalent inductance of the RF-SQUID is influenced by the magnetic flux within the SQUID loop, which is modulated by the current signal flowing through the TES. Variations in the RF-SQUID's equivalent inductance result in changes in the resonant frequency and transmission parameters of the series-connected quarter-wavelength resonator. Consequently, measuring the changes in the resonator's frequency or transmission parameters can be utilized to measured the TES signal. The resonant frequencies of the quarter-wavelength resonators in each channel differ, enabling multiple channels at distinct frequencies to be read out simultaneously through the common CPW feedline. Additionally, all RF-SQUIDs are linked to a common modulation line that linearizes their responses through flux ramp modulation.

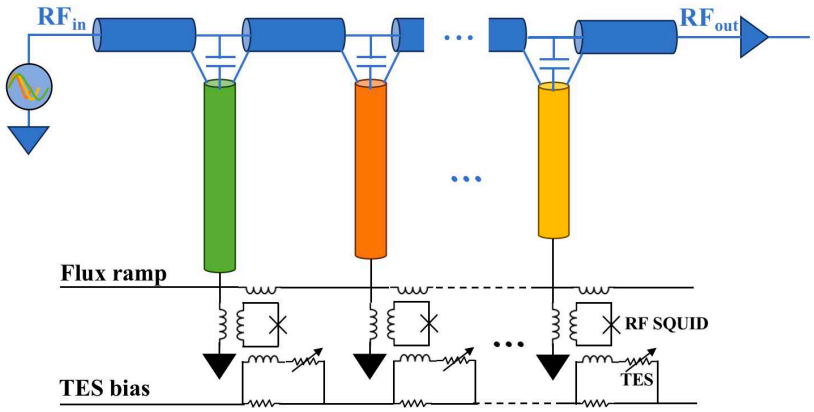


Fig. 1: The equivalent electronics schematic diagram of μMux

Fig. 2 presents a microphotograph of the 32-channel microwave SQUID multiplexer designed and fabricated at the Institute of High Energy Physics (IHEP), Chinese Academy of Sciences. The layout of the prototype is shown as Fig. 2(a). The frequency spacing for the 32 channels is set to 10 MHz. These channels are categorized into four groups, with each group comprising eight channels (e.g., 1-1, 1-2, ..., 1-8), each spaced 10 MHz apart from neighboring frequencies. The frequency interval between adjacent channels in the geometric distribution (e.g., 1-1 and 2-1, 2-1 and 3-1) is 80 MHz, which helps prevent cross-talk among different channels. The 32-channel μMux incorporates four flux ramp lines, each capable of modulating eight RF-SQUIDs. Each

flux ramp includes two corresponding bonding pads for testing. Fig. 2(b) illustrates the microscope image of the chip. The resonator (shown in Fig. 2(b)) is constructed from 200 nm thick niobium (Nb) and features a central conductor width of 9 μm. The slot width between this central conductor and the ground is 6 μm. All resonators are capacitively coupled to a common CPW feedline, which has a center conductor width of 15 μm and a gap of 10 μm from the ground. To achieve this coupling, the resonator operates parallel to the feedline CPW over a specific length (as depicted in Fig. 2(c)), allowing for capacitive coupling. The quality factor can be adjusted by modifying the coupling length or spacing.

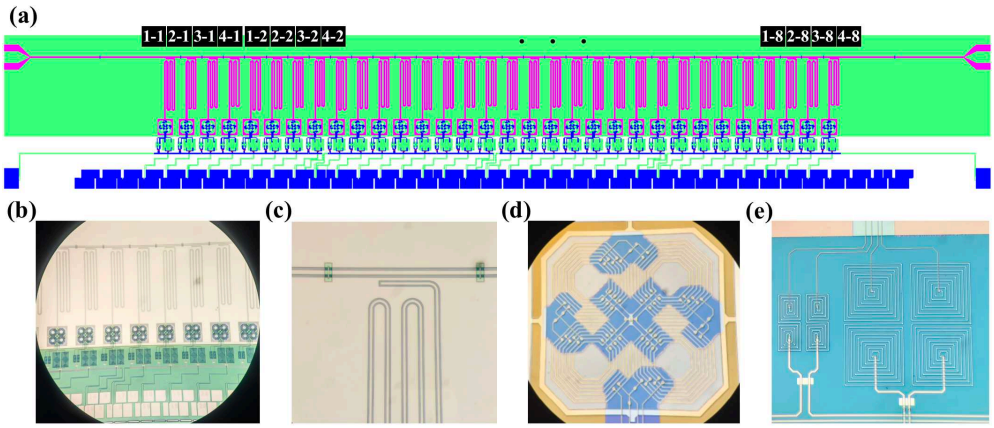


Fig. 2: (a) Design of μMux; (b) Partial microphotograph of the chip; (c) Quarter-wavelength resonator with capacitively coupled to the feedline; (d) RF-SQUID and slotting washer; (e) Flux ramp LR filter (left) and input coil LR filter (right).

Table 1: The simulated inductances and mutual inductances of μMux.

Inductance (pH)	SQUID	Input coil	Flux ramp coil	Resonator
SQUID	42.3	228.9	50.9	2.0
Input coil		4144.7	292.3	18.6
Flux ramp coil			882.6	5.42
Resonator				161.5

Each resonator is inductively coupled to the RF-SQUID. The RF-SQUID is designed as a second-order gradiometric with 4 loops to reduce magnetic interference. Each loop is an octagonal slotted washer. The linewidth of slotted-washer and coils is designed to be as narrow as 3 μm to reduce the the probability of flux-trapping. μMux employs flux ramp modulation to linearize the input coil response. A flux ramp coil is added to the slotted washer and the direction of the flux-ramp coil is made consistent

with that of the input coil. The inductances and mutual inductances of each part are calculated based on InductEx [20] as shown in Table 1. The microwave excitation signal in the CPW feedline may couple inductively and enter the bias circuit of TES via the input coil. This would cause a change in the bias state of TES and thereby affect the readout system noise. Therefore, an LR low-pass filter is added between the input coil and TES (shown as in Fig. 2(e)).

3 Fabrication of the microwave SQUID multiplexer

The μMux prototype was fabricated at the superconducting micro-nano processing platform at IHEP. To manufacture the μMux, we combined a high-quality Josephson tunnel junction fabrication process with the production of superconducting microwave resonators that possess high internal quality factors. Fig. 3 presents the test results of a 4 μm $\times$ 4 μm Josephson junction created in our laboratory. The junction was measured at 3.8 K inside a pulse-tube cryostat. From the measured I-V curve, a gap current (I_g) of 2 μA is extracted. Using the relation $I_c = \pi\ I_g/4$, the critical current density (J_c) is calculated to be approximately 0.098 $\mu A/(\mu m)^2$. Due to such a low J_c, the actual critical current (I_c) is incredibly small and therefore not directly discernible in the I-V curve. This suppression is primarily attributed to the high sensitivity of small critical currents to external electromagnetic interference.

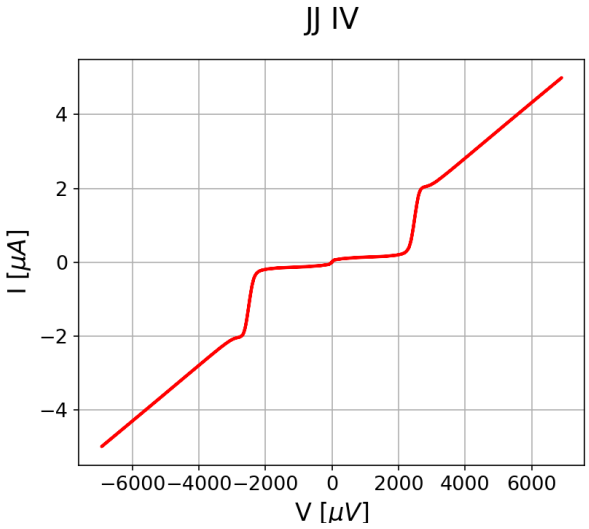


Fig. 3: The measured IV curve of a 4 μm $\times$ 4 μm Josephson junction

Fig. 4 illustrates the manufacturing process of the μMux, which involves ten photo-lithographies, seven dry etchings, one lift-off, two wet etchings, and several deposition steps. Firstly, a trilayer film of Nb/Al-AlO_x/Nb (200 nm/14 nm/150 nm) was sputtered onto a 4-inch high-resistance silicon substrate using magnetron sputtering. The upper Nb layer was defined as the junction region using Inductively Coupled

Plasma Reactive Ion Etching (ICP-RIE). This junction region was then protected by anodization, followed by Ion Beam Etching (IBE) of the oxide layer. The bottom superconducting Nb layer was etched in two steps. Firstly, Reactive Ion Etching (RIE) was employed to form the conductor wire. Subsequently, the Nb layer was etched again using ICP-RIE to create the CPW feedline and the quarter-wavelength CPW resonator. A 350 nm thick SiO_2 isolation layer was deposited using low-temperature Inductively Coupled Plasma Chemical Vapor Deposition (ICP-CVD) and subsequently etched to form vias. An additional Nb layer was sputtered to act as the conductor layer, connecting the Josephson junction, input coil, flux ramp modulation coil, and LR filter, as well as leading to the pads. Next, the resistive layer was deposited by electron beam evaporation (the material was Ti/Pd). Finally, the SiO_2 in the gaps of the CPW and SQUID was removed through wet etching.

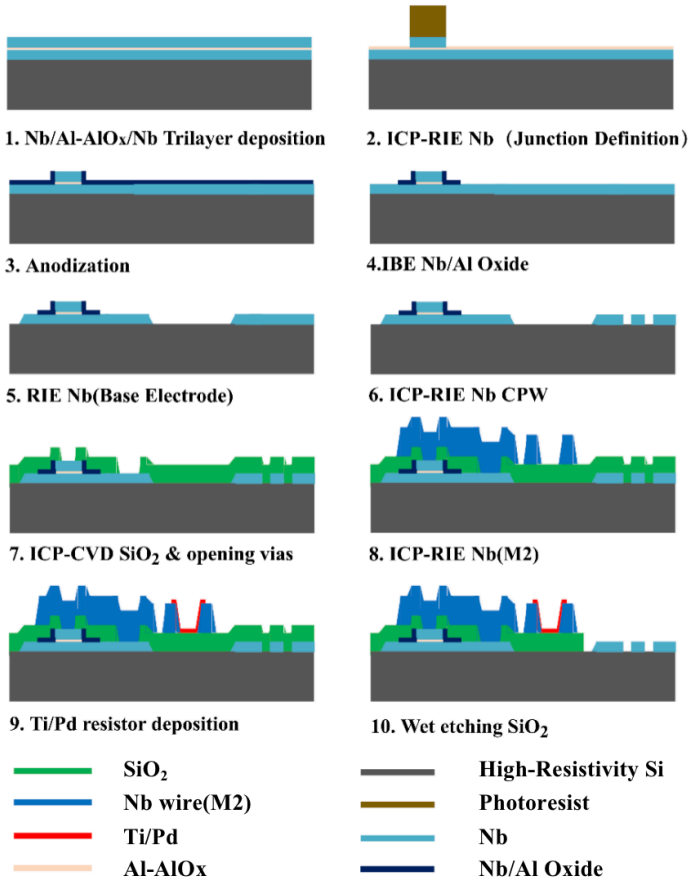


Fig. 4: The fabrication procedure of μMux

4 Experimental setup for the microwave SQUID multiplexer prototype

The overall test block diagram of the μMux is illustrated in Fig. 5. This system allows us to obtain the S_{21} transmission parameters and noise information of the μMux chip. The μMux sample is installed in an adiabatic demagnetization refrigerator (ADR). Depending on the operating temperature, the readout electronics are divided into cryogenic readout electronics located inside the refrigerator and room-temperature readout electronics situated outside. Fig. 5(a) depicts the cryogenic section, which includes a signal generator used to produce the flux-ramp signal. Fig. 5(b) illustrates the room-temperature readout electronics. The cryogenic readout electronics consist of a Low-Noise Amplifier (LNA), attenuator, circulator, and flux-ramp cables. This configuration reduces the excitation power of the comb-like spectrum generated by the room-temperature readout electronics to an appropriate level, aligning with the requirements of the μMux resonators. Additionally, it lowers the noise temperature at the input end of the μMux chip. The modulated comb spectrum output from the μMux chip is then amplified by the LNA to an appropriate power level, ensuring compatibility with the readout requirements of the room-temperature electronics. The room-temperature readout section mainly comprises a fast Analog Digital Converter(ADC)/Digital Analog Converter(DAC) board, an intermediate frequency (IF) board, and an IF board control board, among other components.

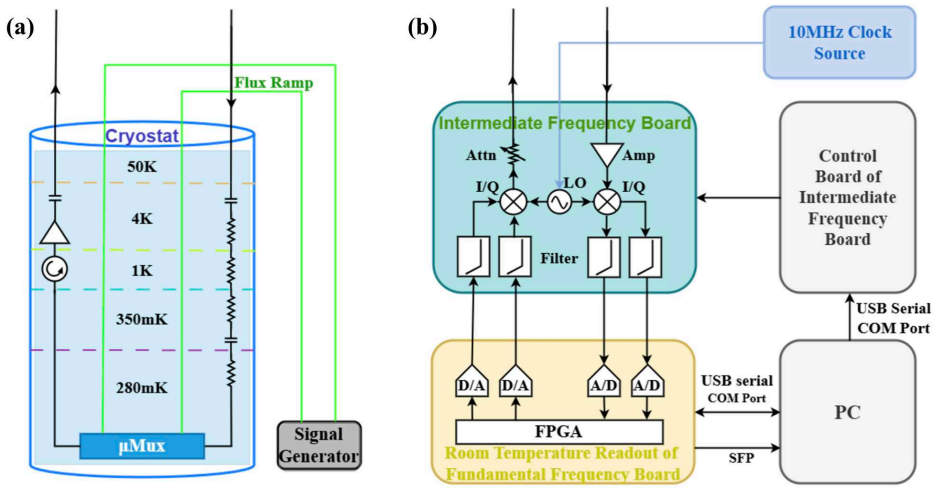


Fig. 5: Block diagram of μMux readout electronics. (a) The cryogenic readout electronics; (b) The room-temperature readout electronics.

The main characterization measurement of μMux include magnetic flux dependent measurements of the resonator's resonant frequency f_r, the internal quality factor Q_i

and the coupling quality factor Q_c. Therefore, we measured the transmission parameters S_{21} of various magnetic fluxes passing through the SQUID loop. By changing the current of the flux ramp coil, the magnetic flux of eight channels in the same flux ramp line was simultaneously altered. We used the algorithm described in [21] to extract f_r, Q_i and Q_c from the measured data.

5 Results

5.1 Resonance frequency measurement

For the initial characterization of the microwave SQUID multiplexer, we measured the S_{21} parameter of the device using a vector network analyzer for resonance frequency searching. The S_{21} measurements were conducted with excitation powers of -10 dBm and -30 dBm, respectively, at a temperature of 60 mK. Fig. 6 displays the measured transmission parameters of the microwave SQUID multiplexer prototype. The eight channels highlighted within the red box in the μMux layout of Fig. 6 were measured in detail. These channels are labeled as ch01 to ch07, as shown in Fig. 6, with the exception of one missing highest resonant frequency. When measuring the resonant frequencies of the seven channels, we performed a detailed S_{21} measurement for these channels under different magnetic fluxes applied by the flux ramp coil.

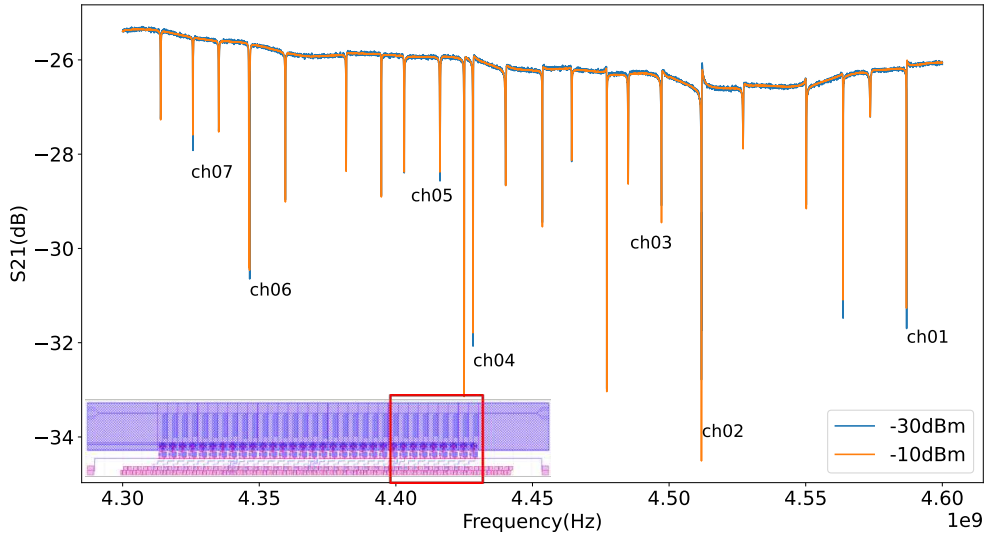


Fig. 6: Measured S_{21} of the μMux prototype. The measurement was conducted at 60 mK using a vector network analyzer, with the excitation powers being -10 dBm and -30 dBm respectively.

Fig. 7 shows the S_{21} parameters of a single channel under different magnetic fluxes passing through the corresponding SQUID loop, it can be seen that when the magnetic flux passing through the SQUID loop changes, the resonant frequency shifts.

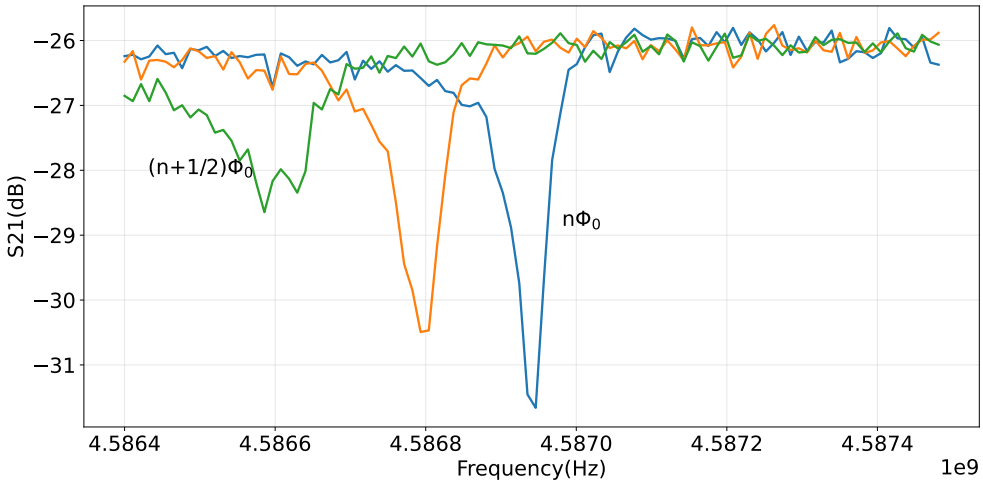


Fig. 7: Measured S_{21} parameters of a single channel with different magnetic fluxes in SQUID loop

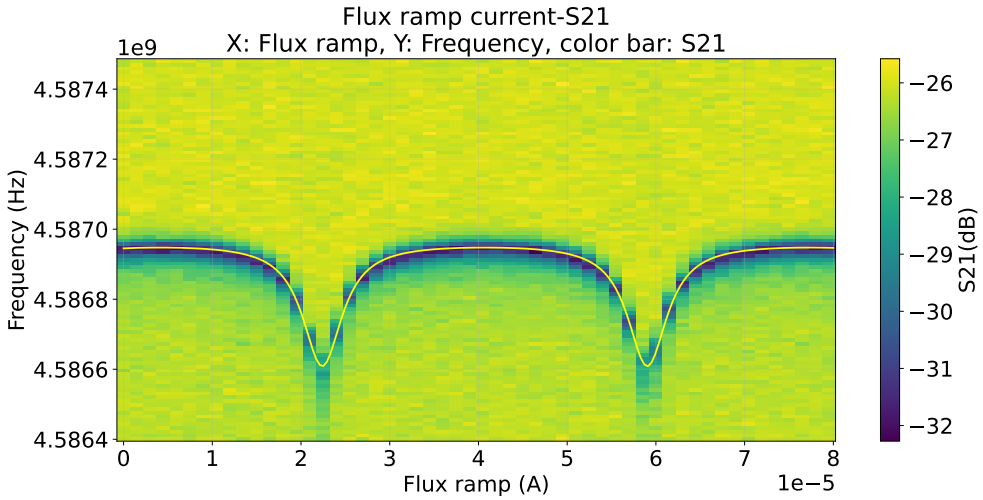


Fig. 8: Measured S_{21} of ch01 under different flux ramp currents. The determined resonance frequency as well as a fit(the yellow curve) according to [21] are shown in the plot.

To characterize the magnetic flux dependence of the resonant frequency $f_r(\Phi)$, different currents are applied to the flux ramp coil, generating varying magnetic fluxes in the SQUID loop. The measured S_{21} parameters of ch01 under different flux ramp currents are shown in Fig. 8. The test was conducted at 45 mK with an excitation power of -35 dBm. Fig. 9 illustrates the dependence of the resonant frequency on the

flux ramp current ($f_r(I_{mod})$) along with the fitting of this curve based on Equation (2). Equation (1) provides the expression for the resonant frequency under the assumption that the RF-SQUID behaves as a flux-dependent inductance; the relationship between the resonant frequency and flux ramp current is described by Equation (2) and derived from Equation (1), where $\phi = 2\pi M_{mod,eff} I_{mod}/\Phi_0 + \phi_{offset}$.

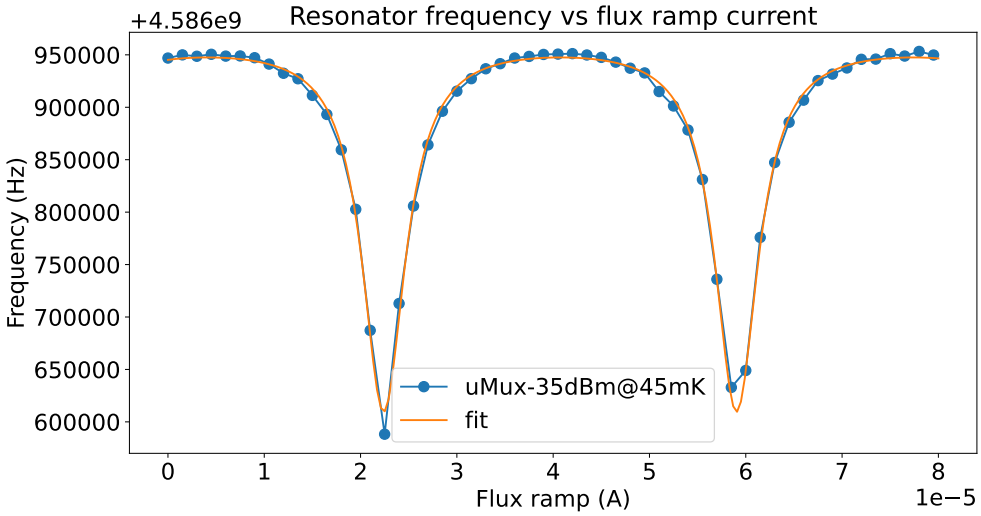


Fig. 9: Dependence of resonant frequency on flux ramp current and curve fitting (ch01). The characterization was conducted at 45 mK with an excitation power of -35 dBm.

$$f_r \approx f_0 - 4f_0^2 C_C Z_0 - \frac{4f_0^2}{Z_0}(L_T - \frac{M_T^2}{L_S}\frac{\lambda\cos\phi}{1+\lambda\cos\phi}) \tag{1}$$

$$f_r(\Phi) = f_{r,off} + \Delta f_{r,mod}\frac{\lambda\cos\phi}{1+\lambda\cos\phi} \tag{2}$$

Here, ϕ_{offset} represents the normalized magnetic flux offset passing through the SQUID loop. Due to parasitic coupling between the flux ramp coil and the input coil, we utilize the effective mutual inductance $M_{\text{mod,eff}}$. The fitting results accurately describe our measurement outcomes. We can determine the flux-independent term in the resonant frequency expression $f_{r,\text{off}} \equiv f_0 - 4f_0^2 C_C Z_0 - \frac{4f_0^2 L_T}{Z_0}$, the modulation coefficient $\Delta f_{r,\text{mod}} \equiv \frac{4f_0^2 M_T^2}{Z_0 L_S}$, the hysteresis parameter λ, and the effective mutual inductance $M_{\text{mod,eff}}$. We conducted this analysis for all seven measured channels. Table 2 summarizes the relevant parameters obtained from the fitting of these channels. The results indicate that the measured values of the effective mutual inductance coefficients for different channels are generally consistent, with a deviation from simulation values within 12%. The hysteresis parameter λ ranges approximately from 0.6 to 0.9,

appearing somewhat random. Using the calculated value of the shielded SQUID inductance L_S, we find the critical current to range from 4.6 to 6.9 μA. This is close to our expected critical current, though it shows variability. This variability may arise from processing the chips using 4-inch wafers, which could lead to differences in the Josephson junction currents at various positions on the chips.

Table 2: Summary of fitting parameters for the measured 7 channels.

Channel	f_r/GHz	λ	$M_{\mathrm{mod,eff}}$/pH
1	4.5869	0.901	56.42
2	4.5120	0.618	56.79
3	4.4973	0.913	56.35
4	4.4283	0.909	56.39
5	4.4162	0.913	56.21
6	4.3465	0.707	56.26
7	4.3352	0.714	56.36

5.2 Quality factor measurement

The internal quality factor of the microwave resonator is related to the magnetic flux Φ passing through the SQUID loop. To investigate this effect, Fig. 10 presents the relationship between the measured internal quality factor Q_i, extracted from ch01 during the resonance curve fitting process, and the flux ramp current. The tests were conducted at 45 mK with an excitation power of -35 dBm. It is evident that Q_i and the flux ramp current exhibit a periodic dependence, with the period matching that of the resonant frequency's dependence on the flux ramp current. According to the multiplexer model, periodic modulation of the flux ramp current is expected when the sub-gap resistance of the Josephson junction is small. Therefore, we use the following formula for fitting:

$$\frac{1}{Q_i} = \frac{1}{Q_{\mathrm{offset}}} + \left(\frac{\pi Z_0 R_{sg} (1 + \lambda \cos\phi)^2}{4(\omega M_T)^2} \right)^{-1} \tag{3}$$

Here, Q_{offset} represents the offset of the internal quality factor, incorporating all contributions that are independent of the magnetic flux. R_{sg} is the sub-gap resistance of the Josephson junction. During the fitting process, Q_{offset} and R_{sg} are the only fitting parameters, as we fixed λ to the value obtained from fitting the dependence of the resonant frequency on the flux ramp current. It can be observed that there is a strong consistency between the measured internal quality factor and the fitted model. Based on the test results of our seven channels, the value of the sub-gap resistance R_{sg} ranges from 60 Ω to 1160 Ω. This is significantly lower compared to the sub-gap resistance value of high-quality Nb/Al-AlO$_x$/Nb junctions. This discrepancy is likely due to deviations in the optimal sputtering parameters necessary for achieving low intrinsic stress in the Josephson junction or damage caused by the etching process. We remain optimistic about resolving this issue in the future.

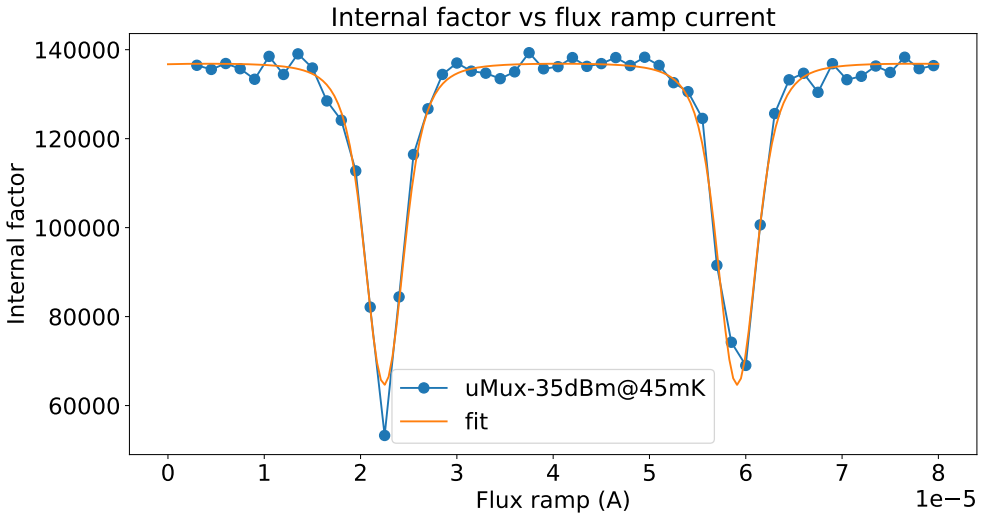


Fig. 10: The dependence of the internal quality factor Q_i of ch01 on the flux ramp current. The measurement was carried out at a temperature of 45 mK, using an excitation power of -35 dBm. The solid orange line is the fitting based on formula (3), assuming that the internal quality factor is affected by the sub-gap resistance of the Josephson junction.

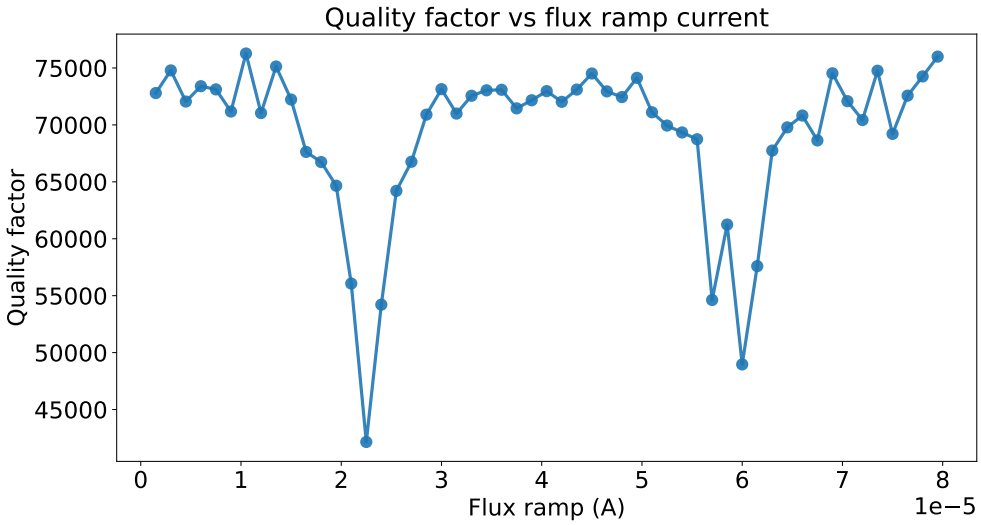


Fig. 11: The dependence of the measured quality factor Q of ch01 on the flux ramp current

The internal quality factor of each channel has a periodic dependence on the flux ramp current. While the coupling quality factor is fixed, it is related to the coupling length and coupling spacing between the resonator and the feedline, and is not affected by the flux ramp current. Therefore, the quality factor of each channel also has a certain dependence on the flux ramp current. Fig. 11 shows the dependence of the quality factor Q measured in ch01 on the flux ramp current. It can be seen that the dependence of Q on the flux ramp current is similar to that of Q_i on the flux ramp current. Table 3 presents a summary of the quality factors for the measured seven channels.

Table 3: Summary of measured quality factors for the measured seven channels.

Channel	Q_i	Q_c	Q
1	137261	161098	73000
2	123651	129359	64921
3	46483	95269	30091
4	100269	88366	40838
5	33293	88358	22569
6	118264	94487	45457
7	33267	131713	26559

5.3 Flux modulation and readout noise measurement

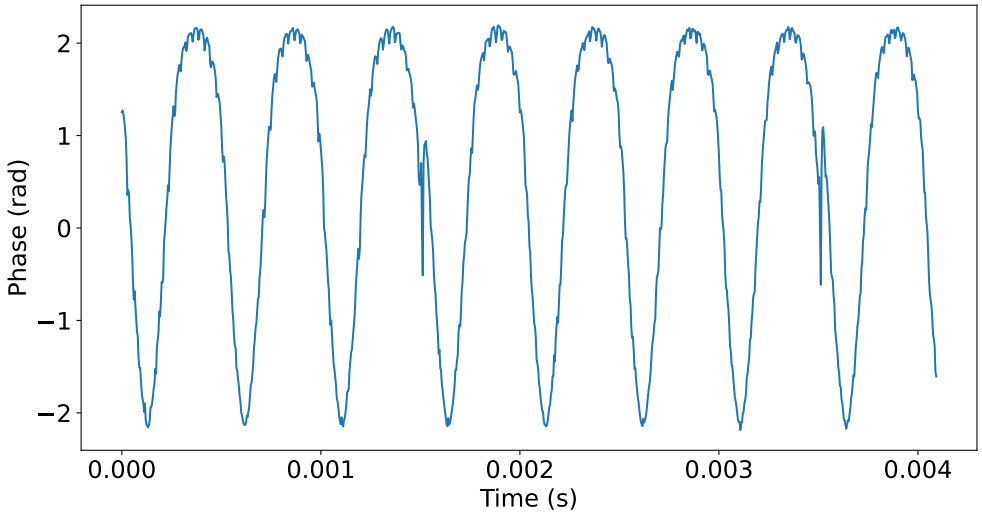


Fig. 12: Modulation curve

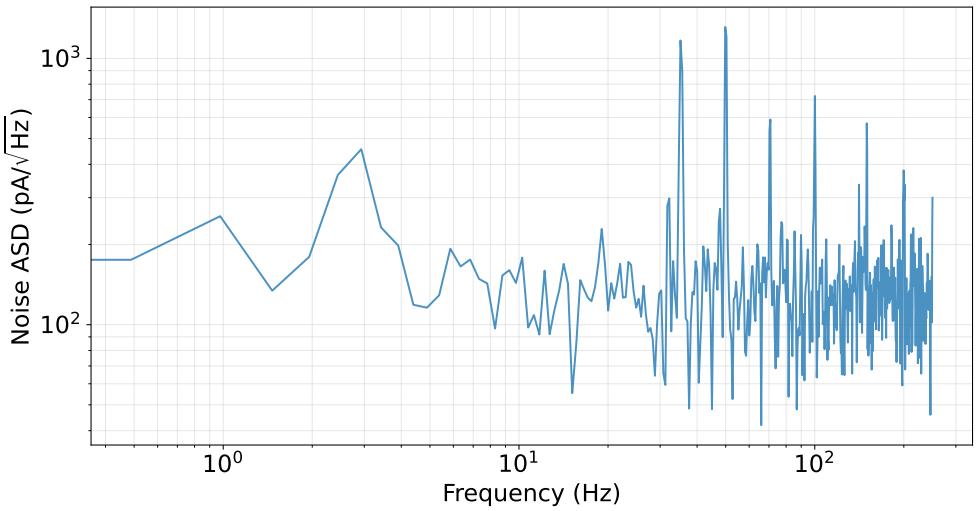


Fig. 13: Measured equivalent noise current (NEI) of ch01

By supplying a sawtooth wave signal to the flux ramp coil through a signal generator, the noise performance of the μMux can be assessed. The excitation tone signals for reading out the seven channels of the μMux prototype are generated and combined by the room-temperature electronics. The frequencies of the generated tone signals are derived from the fitted results of the measured S_{21}. The demodulated phase signal of the flux ramp modulation is illustrated in Figure 12. From this demodulated phase signal, we can extract the signal from the input coil of the μMux. When no signal is input from the input coil, the demodulated signal can be utilized to derive the equivalent noise current using Fast Fourier Transform (FFT) analysis. The measured equivalent noise current power for ch01 is presented in Figure 13. It can be observed that the measured equivalent noise current (NEI) is 154 pA/$\sqrt{\text{Hz}}$ in the frequency range of 2–20 Hz.

6 Conclusion

We fabricated a 32-channel microwave SQUID multiplexer prototype and tested eight channels. Among these, seven channels exhibited magnetic flux-modulated responses. The measured equivalent noise current reached 154 pA/$\sqrt{Hz}$ and the quality factor was 73,000. While challenges remain, such as the lack of resonance points and inconsistencies in the critical current of the Josephson junctions, we plan to investigate and resolve these issues. By optimizing the etching conditions and the stress during film deposition, we anticipate that these problems will be addressed. Furthermore, we aim to fabricate and characterize a μMux prototype with a higher multiplexing ratio, which will be utilized for the upgrade of AliCPT.

Funding This work is supported by the National Key Research and Development Program of China (Grant No.2021YFC2203401), Scientific Instrument Developing

Project of the Chinese Academy of Sciences (Grant No.YJKYYQ20190065), Youth Innovation Promotion Association CAS 2021011, Open Research Fund of the State Key Laboratory of Particle Astrophysics (Grant No. 2025000276).

References

[1] J. Clarke, A.I. Braginski, *The SQUID handbook: volume 1* (2004)

[2] K.N. Abazajian, P. Adshead, Z. Ahmed, S.W. Allen, D. Alonso, K.S. Arnoldand, et al., *CMB-S4 Science Book, First Edition* (2016). https://doi.org/10.2172/1352047

[3] W.B. Doriese, K.M. Morgan, D.A. Bennett, et al., Developments in Time-Division Multiplexing of X-ray Transition-Edge Sensors. Journal of Low Temperature Physics **184**, 389–395 (2016). https://doi.org/10.1007/s10909-015-1373-z

[4] S.W. Henderson, J.R. Stevens, M. Amiri, J. Austermann, J.A. Beall, S. Chaudhuri, H.M. Cho, S.K. Choi, N.F. Cothard, K.T. Crowley, S.M. Duff, C.P. Fitzgerald, P.A. Gallardo, M. Halpern, M. Hasselfield, G. Hilton, S.P.P. Ho, J. Hubmayr, K.D. Irwin, B.J. Koopman, D. Li, Y. Li, J. McMahon, F. Nati, M. Niemack, C.D. Reintsema, M. Salatino, A. Schillaci, B.L. Schmitt, S.M. Simon, S.T. Staggs, E.M. Vavagiakis, J.T. Ward, *Readout of two-kilopixel transition-edge sensor arrays for Advanced ACTPol*, in *Millimeter, Submillimeter, and Far-Infrared Detectors and Instrumentation for Astronomy VIII*, vol. 9914, ed. by W.S. Holland, J. Zmuidzinas. International Society for Optics and Photonics (SPIE, 2016), p. 99141G. https://doi.org/10.1117/12.2233895

[5] M. Durkin, J.S. Adams, S.R. Bandler, J.A. Chervenak, E.V. Denison, W.B. Doriese, S.M. Duff, F.M. Finkbeiner, J.W. Fowler, J.D. Gard, G.C. Hilton, R. Hummatov, K.D. Irwin, Y.I. Joe, R.L. Kelley, C.A. Kilbourne, A.R. Miniussi, K.M. Morgan, G.C. O'Neil, C.G. Pappas, F.S. Porter, C.D. Reintsema, D.A. Rudman, K. Sakai, S.J. Smith, R.W. Stevens, D.S. Swetz, P. Szypryt, J.N. Ullom, L.R. Vale, N. Wakeham, Mitigation of Finite Bandwidth Effects in Time-Division-Multiplexed SQUID Readout of TES arrays. IEEE Transactions on Applied Superconductivity **31**(5), 1–5 (2021). https://doi.org/10.1109/TASC.2021.3065279

[6] D.C. Goldfinger, Z. Ahmed, D.R. Barron, W.B. Doriese, M. Durkin, J.P. Filippini, G. Haller, S.W. Henderson, R. Herbst, J. Hubmayr, K. Irwin, B. Reese, L. Sapozhnikov, K.L. Thompson, J. Ullom, M.R. Vissers, End-to-End Modeling of the TDM Readout System for CMB-S4. Journal of Low Temperature Physics **215**(3), 143–152 (2024). https://doi.org/10.1007/s10909-024-03077-2

[7] K. Hattori, Y. Akiba, K. Arnold, D. Barron, A.N. Bender, A. Cukierman, T.d. Haan, M. Dobbs, T. Elleflot, M. Hasegawa, M. Hazumi, W. Holzapfel, Y. Hori, B. Keating, A. Kusaka, A. Lee, J. Montgomery, K. Rotermund, I. Shirley, A. Suzuki, N. Whitehorn, Development of Readout Electronics

for POLARBEAR-2 Cosmic Microwave Background Experiment. Journal of Low Temperature Physics **184**, 512–518 (2016). https://doi.org/10.1007/s10909-015-1448-x

[8] D. Vaccaro, H. Akamatsu, L. Gottardi, M.d. Wit, M.P. Bruijn, J.v.d. Kuur, K. Nagayoshi, E. Taralli, K. Ravensberg, J.R. Gao, J.W.A.d. Herder, Developments on frequency domain multiplexing readout for large arrays of transition-edge sensor x-ray micro-calorimeters. Journal of Low Temperature Physics **216**, 21–28 (2024). https://doi.org/10.1007/s10909-024-03099-w

[9] R.d. Hartog, B.J.v. Leeuwen, P. Peille, J.v.d. Kuur, L. Ravera, D.v. Loon, B. Jackson, J.W.d. Herder, Performance of a state-of-the-art DAC system for FDM readout. Proc. SPIE 10699, Space Telescopes and Instrumentation 2018: Ultraviolet to Gamma Ray, 106994Q (2018). https://doi.org/10.1117/12.2312793

[10] K.D. Irwin, M.D. Niemack, J. Beyer, H.M. Cho, W.B. Doriese, G.C. Hilton, et al., Code-division multiplexing of superconducting transition-edge sensor arrays. Superconductor Science and Technology **23**(3), 034004 (2010). https://doi.org/10.1088/0953-2048/23/3/034004

[11] K.M. Morgan, B.K. Alpert, D.A. Bennett, E.V. Denison, W.B. Doriese, J.W. Fowler, J.D. Gard, G.C. Hilton, K.D. Irwin, Y.I. Joe, et al., Code-division multiplexed read-out of large arrays of tes microcalorimeters. Applied Physics Letters **109**, 112604 (2016). https://doi.org/10.1063/1.4962636

[12] K.D. Irwin, K.W. Lehnert, Microwave SQUID multiplexer. Applied Physics Letters **85**(11), 2107–2109 (2004). https://doi.org/10.1063/1.1791733

[13] C. Yu, Z. Ahmed, J.C. Frisch, S.W. Henderson, M. Silva-Feaver, K. Arnold, D. Brown, J. Connors, A.J. Cukierman, J.M. DEwart, B.J. Dober, J.E. Dusatko, G. Haller, R. Herbst, G.C. Hilton, J. Hubmayr, K.D. Irwin, et al., SLAC microresonator RF(SMuRF) electronics: A tone-tracking readout system for superconducting microwave resonator arrays. Review of Scientific Instruments **94**, 014712 (2023). https://doi.org/10.1063/5.0125084

[14] B. Dober, Z. Ahmed, K. Arnold, D.T. Becker, D.A. Bennett, J.A. Connors, A. Cukierman, J.M. D'Ewart, S.M. Duff, J.E. Dusatko, J.C. Frisch, J.D. Gard, S.W. Henderson, R. Herbst, G.C. Hilton, et al., A microwave SQUID multiplexer optimized for bolometric applications. Applied Physics Letters **118**, 062601 (2021). https://doi.org/10.1063/5.0033416

[15] J.C. Groh, Z. Ahmed, J. Austermann, J. Beall, D. Daniel, S.M. Duff, S.W. Henderson, J. Hubmayr, R. Lew, M. Link, T.J. Lucas, J.A.B. Mates, M. Silva-Feaver, R. Singh, J. Ullom, L. Vale, J. Van Lanen, M. Vissers, C. Yu, Demonstration of a 1820 channel multiplexer for transition- edge sensor bolometers. Applied Physics Letters **127**, 152602 (2025). https://doi.org/10.1063/5.0290914

[16] A. Cukierman, Z. Ahmed, S. Henderson, E. Young, C. Yu, D. Barkats, D. Brown, S. Chaudhuri, J. Cornelison, J.M. DEwart, M. Dierickx, B.J. Dober, J. Dusatko, S. Fatigoni, J.P. Filippini, J.C. Frisch, G. Haller, M. Halpern, G.C. Hilton, J. Hubmayr, K.D. Irwin, et al., Microwave multiplexing on the Keck Array. Journal of Low Temperature Physics **199**, 858–866 (2019). https://doi.org/10.1007/s10909-019-02296-2

[17] Y. Li, K. Arnold, Z. Atkins, S.M. Bruno, N.F. Cothard, B. Dober, C.J. Duell, S.M. Duff, P.A. Gallardo, E. Healy, S.P. Ho, J. Hubmayr, B. Keating, A.T. Lee, A. Mangu, H. McCarrick, M.D. Niemack, L. Newburgh, C. Raum, M. Salatino, T. Sasse, M. Silva-Feaver, S.M. Simon, S. Staggs, et al., Assembly and Integration Process of the High-Density Detector Array Readout Modules for the Simons Observatory. Journal of Low Temperature Physics **199**, 985–993 (2020). https://doi.org/10.1007/s10909-020-02386-6

[18] M. Salatino, J. Austermann, K.L. Thompson, P.A.R. Ade, X. Bai, J.A. Beall, D.T. Becker, Y. Cai, Z. Chang, D. Chen, J. Connors, P. Chen, B. Dober, J. Delabrouille, S.M. Duff, G. Gao, R.C. Givhan, S. Ghosh, G. Hilton, B. Hu, J. Hubmayr, E. Karpel, C.L. Kuo, H. Li, M. Li, S.Y. Li, X. Li, M. Link, Y. Li, H. Liu, L. Liu, Y. Liu, F. Lu, T. Lucas, X. Lu, J.A.B. Mates, et al., The Design of the Ali CMB Polarization Telescope receiver. Millimeter, Submillimeter, and Far-Infrared Detectors and Instrumentation for Astronomy X p. 114532A (2020). https://doi.org/10.1117/12.2560709

[19] D. Bennett, J.B. Mates, S. Bandler, D. Becker, J. Fowler, J. Gard, G. Hilton, K. Irwin, K. Morgan, C. Reintsema, K. Sakai, D. Schmidt, S. Smith, D. Swetz, J. Ullom, L. Vale, A. Wessels, Microwave SQUID multiplexing for the Lynx x-ray microcalorimeter. Journal of Astronomical Telescopes, Instruments, and Systems **5(2)**, 021007 (2019). https://doi.org/10.1117/1.JATIS.5.2.021007

[20] C.J. Fourie. Inductex software. https://www.inductex.info (2015)

[21] J.S. Gao, The Physics of Superconducting Microwave Resonators. Thesis, California Institute of Technology (2008)